Modeling of Defect Evolution and TED under Stress based on DFT Calculations

Hsiu-Wu Guo and Scott T. Dunham
Department of Electrical Engineering
University of Washington
Seattle, Washington 98195, USA
Email: hwg@u.washington.edu
dunham@ee.washington.edu

Chen-Luen Shih
Department of Materials Science and Engineering
University of Washington
Seattle, Washington 98195, USA
Email: chen-luen.shih@intel.com

Chihak Ahn
Department of Physics
University of Washington
Seattle, Washington 98195, USA
Email: chahn@u.washington.edu

***Abstract*— The incorporation of strain in order to improve mobility has become an important element in CMOS device scaling. In this work, we have developed a new moment-based model of extended defect kinetics and further studied the impact due to stress on the energies of impurities, point defects and particularly extended defects. We specifically look at point defect clusters which control transient enhanced diffusion (TED). The results enable comprehensive models for dependence of nanoscale device structures on stress which can be used for process optimization.**

I. Introduction

The trend of VLSI technology toward nanoscale dimensions includes the incorporation of stress/strain, due to the fact that induced stress can enhance carrier mobility [1]. Stress also has a large impact on transient enhanced diffusion (TED) and dopant activation in ultra-shallow junctions. {311} defects form during TED in silicon due to the excess point defects introduced by the ion implantation. For subamorphizing Si implants, almost the entire net excess interstitials aggregate into these defects within a very short period of time (less than 5 s at 815°C) [2]. Eventually, the interstitials bound to these defects dissolve and disappear as the annealing process continues. Stolk *et al.* [3] have suggested that TED occurs by the emission of silicon self-interstitials from {311} clusters (also called rod-like defects) during the annealing since the measured time scale for dissolution of {311} defects is almost identical to the TED. In addition to {311} defects, Zhang *et al.* [4] and Kim *et al.* [5] reported small clusters of interstitials also play a role in early time phase of the TED.

In this paper, we extend the point defect clustering model developed in previous efforts and utilize *ab-initio* calculations to study stress effects on the formation of point defect clusters which control TED.

II. Kinetic Precipitation Models

The full kinetic precipitation model [6] and reduced moment-based precipitation model (RKPM) [7] were introduced to analyze the dynamic behavior of extended defects in previous efforts. In this work, we adapted RKPM with a delta function approximation to enhance computational efficiency while also giving more physically meaningful parameters.

A. Full Kinetic Precipitation Model

The full kinetic precipitation model (FKPM) [6] describes the evolution of the full precipitate size distribution to account the thermal history effects. Precipitation is driven by the fact that above solubility formation of a separate phase reduces the total free energy of the system. After ion implantation, the supersaturation of interstitials leads to the formation of small I clusters and {311} defects, which control TED. The free energy change upon precipitate formation can be written as:

$$\Delta G_n = -nkT \ln\left(\frac{C_{\mathrm{I}}}{C_{ss}}\right) + \Delta G_n^{excess} \tag{1}$$

where n is the size of the precipitate, C_{I} is the interstitial concentration, and C_{ss} is the solid solubility of interstitials associated with the formation of {311} defects. G_n^{excess} is the excess energy associated with finite sized defects. The precipitation process proceeds by adding interstitials to existing precipitates, which generates a *n*+1 precipitate from a size *n* precipitate. The time evolution of precipitate density can be described as:

$$\begin{aligned} \frac{df_1}{dt} &= -2I_2 - \sum_{n=3} I_n \\ \frac{df_n}{dt} &= I_n - I_{n+1}, \qquad n \geq 2, \end{aligned} \tag{2}$$

where f_n is the precipitate density of size n, and I_n is the flux in precipitate size space from $n-1$ to n. I_n is given by the difference between the growth and dissolution rates, which can be written as:

$$I_n = D_I \lambda_{n-1} (C_{\mathrm{I}} f_{n-1} - C_n^* f_n) \tag{3}$$

where D_I is the diffusivity of interstitals, λ_n is the kinetic growth factor, which can be determined from the interface reaction rate and geometry of the defects [8]. C_n^* is the local equilibrium constant, which is defined such that there is no energy difference with the transition from size $n-1$ to size n ($\Delta G_{n-1} = \Delta G_n$ in Eq. (1)).

$$C_n^* = C_{ss} \exp\left(-\frac{\Delta G_n^{excess} - \Delta G_{n-1}^{excess}}{kT}\right) \tag{4}$$

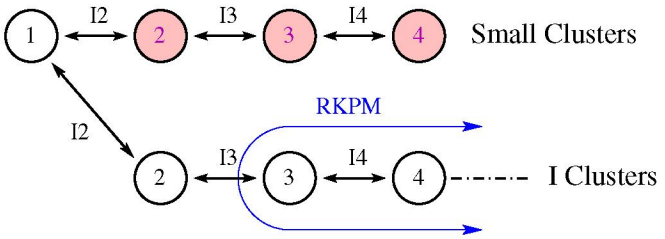

Fig. 1. A schematic shows the concept of RKPM for {311} cluster. FKPM is used for small interstitial clusters, while RKPM describes the behavior of {311} precipitation from size k=3.

B. Reduced Moment-Based Model

Clejan *et al.* [7] introduced reduced moment-based model to enhance the computational efficiency of FKPM. Instead of calculating all the rate equations (Eq. 2) over size space, RKPM keeps track of the lowest moments of the distribution of larger precipitates. Discrete equations are still applied on small clusters shown in Fig. 1. The moments are defined as:

$$m_i = \sum_{n=k}^{\max} n^i f_n \qquad i = 0, 1, ... \tag{5}$$

Note k is the size where RKPM is started as shown in Fig. 1. The rate equations of moments can then be written as:

$$\begin{aligned} \frac{\partial m_i}{\partial t} &= k^i I_k + \sum_{n=k}^{\max}[(n+1)^i - n^i] I_{n+1} \\ &= k^i I_k + D_{\mathrm{I}} m_0 (C_{\mathrm{I}} \gamma_i^+ - C_{ss} \gamma_i^-), \end{aligned} \tag{6}$$

where

$$\begin{aligned} \gamma_i^+ &= \sum_{n=k}^{\max}[(n+1)^i - n^i] \lambda_n \hat{f}_n \\ \gamma_i^- &= \sum_{n=k}^{\max}[n^i - (n-1)^i] \lambda_n \hat{C}^*_{n+1} \hat{f}_{n+1}. \end{aligned} \tag{7}$$

$\hat{f}_n$ is the normalized size distribution ($\hat{f}_n = f_n/m_0$), and $\hat{C}^*_n = C^*_n/C_{ss}$. The first two moments (m_0 and m_1) are considered in this work, therefore, γ_0^-, γ_1^+, and γ_1^- have to be determined.

Note that interstitial small clusters control the early time phase of TED. They are modeled by the discrete equations (Eqs. 2 and 3). In this work, we only include small clusters of size 2, 3, and 4, as larger compact clusters were found to have higher energy than {311} structures [5].

C. RKPM with Delta Function Approximation

We have used FKPM and RKPM to describe the formation of {311} defects. Instead of using analytical approach [9] by assuming the distribution function $\hat{f}_n$ to be given by a non-linear equation, a delta function approximation (DFA) is used. In DFA, the values of both summation terms (γ_1^+ and γ_1^-) are assumed to be equal to the values for a single defect with size equal to the average size in the system ($\hat{m}_1$). This not only simplifies the mathematical procedures for calculating γ_1^- and γ_1^+ in an analytical method but also equips them with more physical meaning. Therefore, Eqs. 7 can be rewritten as:

$$\begin{aligned} \gamma_i^+ &= \lambda_{\hat{m}_1} \hat{f}_{\hat{m}_1} \\ \gamma_i^- &= \lambda_{\hat{m}_1} \hat{C}^*_{\hat{m}_1+1} \hat{f}_{\hat{m}_1}. \end{aligned} \tag{8}$$

III. Comparison between Experimental Data and Simulation Results

In this section, we compare both FKPM and RKPM with DFA to experimental data from Cowern *et al.* [10] (Fig. 2[a]) and Eaglesham *et al.* [11] (Fig. 3). Cowern *et al.* tracked diffusion of a buried boron epitaxy layer after 25keV Si ion implantation with a initial dose $2{\times}10^{13}\mathrm{cm}^{-2}$. Interstitial supersaturation can be obtained, assuming that boron diffuses via interstitials. Eaglesham *et al.* used both plan view and cross sectional transmission electronic microscopy (TEM) to measure the size of {311} interstitial clusters after 40keV Si implantation with dose of $5\mathrm{x}10^{13}\mathrm{cm}^{-2}$. In Fig. 2, both FKPM and RKPM well characterize the time evolution of interstitial supersaturation. At 600°C, TED lasts about five orders of magnitude longer than at 800°C. Good agreement between simulation results and experimental data from Eaglesham *et al.* [11] is shown in Fig. 3.

IV. Prediction of Defect Evolution Under Stress/Strain Conditions

Stress has a significant impact on TED. It changes the small cluster binding energies and effective solubility for {311} defects, as well as the formation and migration energy for point defects. We used the density functional theory (DFT) code VASP [12] with ultrasoft Vanderbilt type pseudopotentials [13] for our calculations. All calculations were performed in general gradient approximation (GGA) with a 64 silicon atom supercell and a 2^3 Monkhorst-Pack **k**-point sampling. The energy cut-off was 250eV. The change in energy due to strain is

$$\Delta E_f(\epsilon) = -\sum_{i=1}^{3}\sum_{j=1}^{3}\sum_{k=1}^{3}\sum_{l=1}^{3} \Omega_0 \Delta\epsilon_{ij} C^{\mathrm{Si}}_{ijkl} \epsilon_{kl} \tag{9}$$

where Ω_0 is volume per lattice site, $\Delta\epsilon_{ij}$ is the induced strain tensor, C_{ijkl} is elastic stiffness tensor, and ϵ_{kl} is the applied strain tensor. The calculated induced strain ($\Delta\epsilon$) for interstitial clusters is shown in Tables I. For the two most important structures, isolated interstitial and {311} defects, asymmetric induced strains were taken into account in calculations. We took the possible {311} plane configuration reported by Kim *et al.* [14] shown in Fig. 4. The induced strain due to other asymmetric interstitial structures (I_3 and I_4) was derived from hydrostatic calculations.

We have used parameters under both tensile and compressive strain conditions to simulate the corresponding behaviors. Both interstitials and interstitial clusters reduce their energy under tensile stress condition. However, clusters (including {311} defects) have a even stronger stress dependence. Thus interstitial clusters are less likely to form under compressive strain conditions and they are more likely to form under tensile

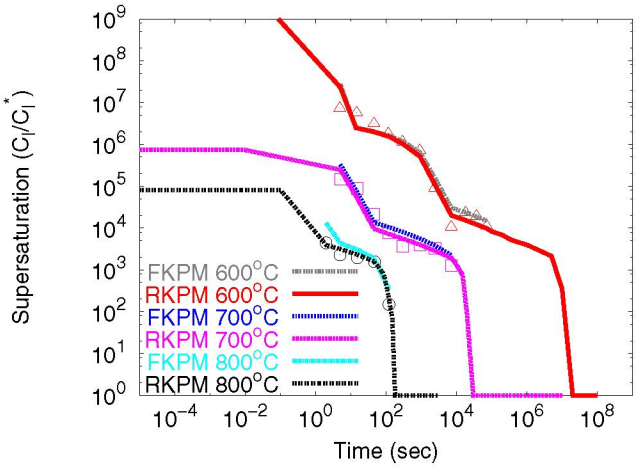

[a]

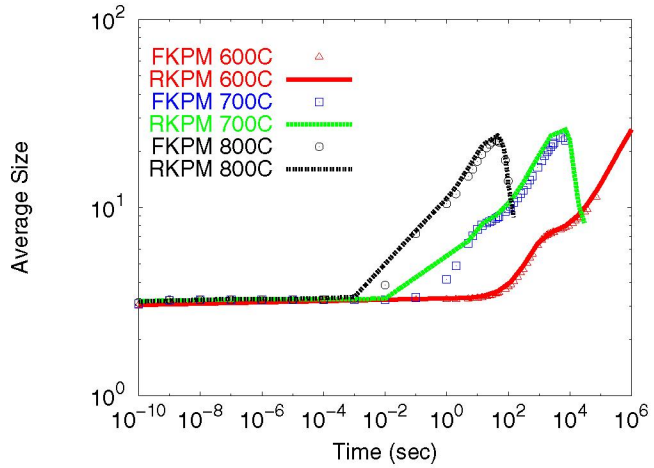

[b]

Fig. 2. [a] Interstitial supersaturation as a function of annealing time and temperature. Symbols represent experimental data reported by Cowern *et al.* [10] and lines are the results from discrete and moment-based models using delta function approximation. [b] Comparison of {311} average size ($\hat{m}_1$) between FKPM and RKPM-DFA under identical implant condition at various anneal temperatures, demonstrating effectiveness of delta function approximation.

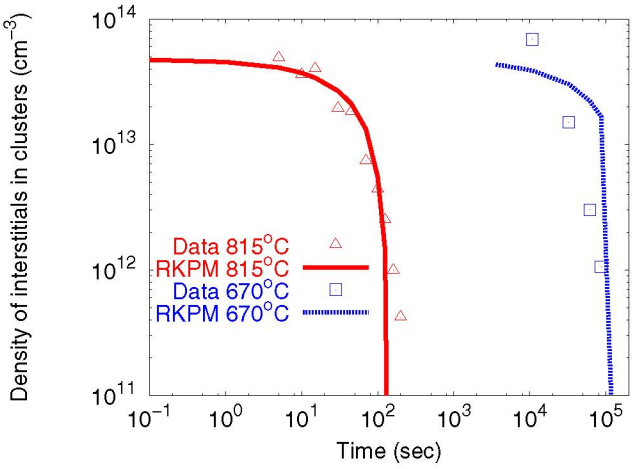

Fig. 3. Time evolution of interstitial density in {311} defects (m_1) and comparison to RKPM. Symbols represent experimental data from Eaglesham *etal.* [11] and lines are the simulation results from moment-based model using delta function approximation.

	I_{split}	I_2	I_3	I_4
$\Delta\epsilon$ (eV)	(0.26, 0.26, 0.047)	0.16	0.36	0.36

	I_{311}		
$\Delta\epsilon$ (eV)	0.29	0.086	0.084
	0.086	0.29	0.086
	0.084	0.086	0.29

TABLE I

INDUCED STRAINS FOR INTERSTITIAL CLUSTERS. FOR TWO KEY STRUCTURES (I AND I_{311}), ASYMMETRY WAS FULLY ACCOUNTED. FOR SINGLE NUMBER INDICATES ALL COMPONENTS OF VECTOR HAVE SAME VALUE.

conditions. Figs. 5[a], [b], and [c] show predictions for I cluster evolution under 1% biaxially tensile/compressive stress compared to stress free condition. Tensile stress favors both small I cluster and {311} formation, giving a longer but less intense TED period, while compressive stress has the opposite effect (higher I concentration but for shorter time). Thus B activation is initially suppressed for compressive stress while I clusters remain, but then recovers more rapidly, with the opposite behavior for tensile stress.

V. CONCLUSION

We were able to describe the evolution of {311} defects using an alternative moment-based model, which possesses excellent computational efficiency and does not require table lookups. This model has been successfully calibrated to give good agreement with the annealing of {311} defects following ion implantation. We also used *ab-initio* calculations to study stress effects on point defect clustering. By including results from first principle calculations into the kinetic precipitation model, predictions show that stress effects play an important role in point defect clustering and dopant activation.

ACKNOWLEDGMENT

This work was supported by Semiconductor Research Corporation (SRC).

REFERENCES

[1] K. Rim, J.L. Hoyt, and J.F Gibbons, IEEE Transactions on Electron Devices **47**, 1406 (2000); J. Welser, J.L. Hoyt, and J.F Gibbons, IEEE Electron Device Letters **15**, 100 (1994).
[2] D.J. Eaglesham, P.A. Stolk, H.-J. Gossmann, and J.M. Poate, Appl. Phys. Lett. **65**, 2305 (1994).
[3] P.A. Stolk, H.-J Gossmann, D.J. Eaglesham, D.C. Jacobson, H.S Luftman, and M. Poate, Beam-Solid Interactions for Materials Synthesis and Characterization Symposium **307**, (1995).
[4] L.H. Zhang, K.S. Jones, P.H. Chi, and D.S. Simon, Appl. Phys. Lett. **67**, 2025 (1995).
[5] J. Kim, F. Kirchho, J. W. Wilkins, and F.S. Khan, Phys. Rev. Let. **84**, 503 (2000).
[6] S.T. Dunham, J. Electrochem. Soc. **142**, 2823 (1995).
[7] I. Clejan and S.T. Dunham, J. Appl. Phys. **78**, 7327 (1995).
[8] S.T. Dunham, Appl. Phys. Lett. **64**, 464 (1993).

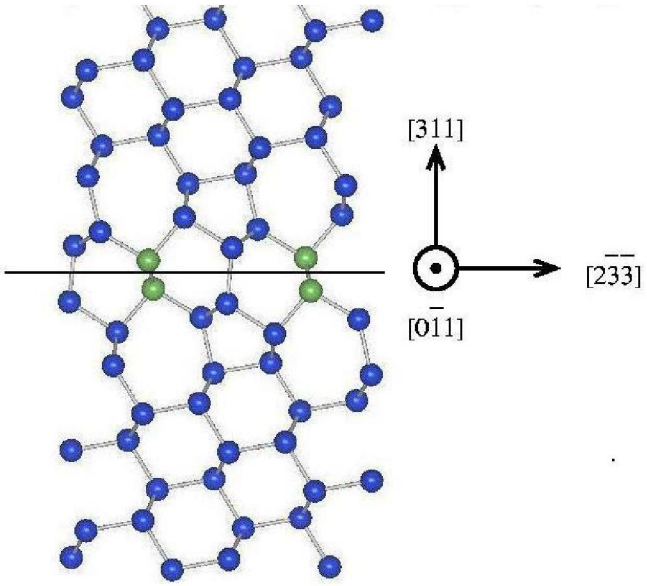

Fig. 4. {311} structure used for *ab-initio* calculation [14].

[9] A. H. Gencer, S. T. Dunham, J. Appl. Phys. **91**, 2883 (2002).

[10] N.E.B. Cowern, G. Mannino, P.A. Stolk, F. Roozeboom, J.G.M. van Barkum, F. Cristiano, A. Claverie, and M. Jaraiz., J. Appl. Phys. **68**, 6191 (1999).

[11] D.J. Eaglesham, P.A. Stolk, H.-J. Gossmann, T.E. Haynes, and J.M. Poate, Nuclear Instruments and Method in Physics Research B **106**, 191 (1995).

[12] G. Kresse, and J. Hafner,Phys. Rev. B **47**, 558 (1993); G. Kresse, and J. Furthmuller, Phys. Rev. B **54**, 11169 (1996).

[13] D. Vanderbilt, Phys. Rev. B **41** 7892 (1990); G. Kresse and J. Hafner, J. Phys. Condens. Matter **6**, 8245 (1994).

[14] J. Kim and J.W. Wilkins, Phys. Rev. B **55**, 16186 (1996).

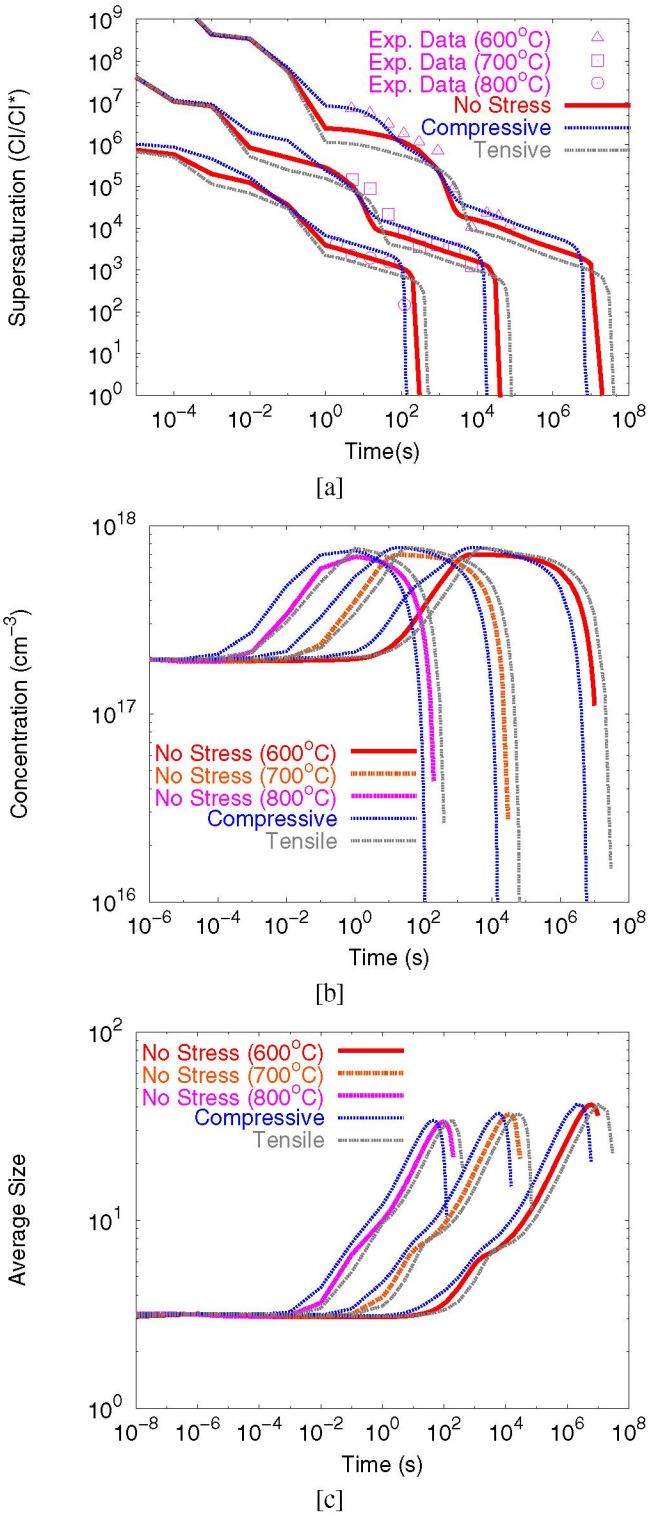

Fig. 5. Simulation result of {311} defect evolution under 1% biaxially tensile/compressive stress compares to stress free condition. (a) Interstitial supersaturation; (b) interstitial concentration in I clusters; (c) {311} defect average size. Supersaturation lasts longer under tensile stress, while I supersaturation is larger for compressive stress.

